Resonance Enhancement in Noise

Cheney, Margaret; Kim, Jerry; Kirsteins, Ivars; Kristensson, Gerhard

2023

Document Version:
Other version

CODEN:LUTEDX/(TEAT-7280)/1-21/(2023)

Resonance Enhancement in Noise

Margaret Cheney, Jerry Kim, Ivars Kirsteins, Gerhard Kristensson

Electromagnetic Theory
Department of Electrical and Information Technology
Lund University
Sweden

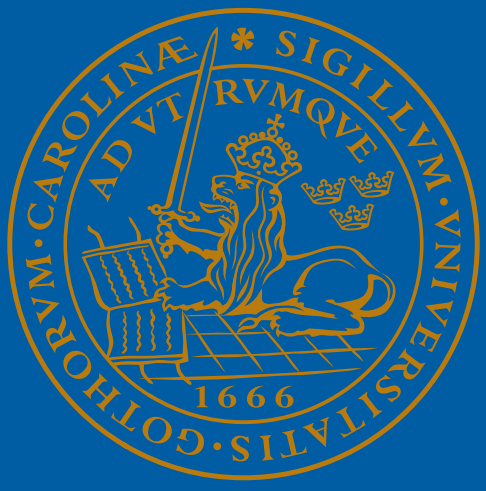

(TEAT-7280)/1-21/(2023): M. Cheney *et al.*, Resonance Enhancement in Noise

Margaret Cheney
cheney@math.colostate.edu

Department of Mathematics and
Department Electrical and Computer Engineering
Colorado State University
1874 Campus Delivery
Fort Collins, CO 80523
USA

Jerry Kim
jkim@envisioneeringinc.com

Envisioneering, Inc.
5904 Richmond Hwy, Ste. 600
Alexandria, VA 22303
USA

Ivars Kirsteins
ivars.p.kirsteins.civ@us.navy.mil

NUWC Division Newport
1176 Howell St.
Newport, RI 02841
USA

Gerhard Kristensson
gerhard.kristensson@eit.lth.se

Department of Electrical and Information Technology
Electromagnetics and Nanoelectronics
Lund University
P.O. Box 118
SE-221 00 Lund
Sweden

Editor: Mats Gustafsson

Abstract

This document compares two approaches to finding resonance peaks from a single sensor: 1) averaging multiple measurements of the transfer function or frequency-domain scattering matrix, versus 2) using the iterative time-reversal process, which involves iteratively re-transmitting a time-reversed version of the scattered field at the previous iterations. The averaging method has the advantage of handling arbitrarily much noise if sufficiently many averages are used. On the other hand, up to a certain level of noise, the time-reversal method has dramatic advantages over the averaging method; but it also requires more complex equipment. This document discusses the tradeoffs involved, with the goal of providing information that may be useful in the system design process.

1 Introduction

For many decades there has been interest in using scattered fields to find target resonances. One reason is for their possible use in target identification [1–4]. Resonant frequencies are connected to the presence, in the complex frequency plane, of poles of the target scattering operator [9,17,23], and the locations of these poles are independent of the aspect angles from which the target is probed. Consequently, identification of target resonances could contribute to the development of an aspect-independent method for identifying a target.

In this paper, the term “resonance" refers simply to a local maximum of the transfer function (frequency-domain scattering matrix). The connection between these peaks and scattering poles was studied further in [17].

This document compares two approaches to finding resonance peaks: 1) averaging multiple measurements of the transfer function and raising it to a power, versus 2) using the iterative time-reversal process. This iterative time-reversal (TR) process [10–12,15,16,20–22] involves first transmitting any signal, receiving the scattered field, time-reversing this scattered field (for example, by sampling the received field, storing it and time-reversing it in a computer), re-transmitting this time-reversed field, and repeating.

In each peak-finding approach, the resulting plot shows a sharp peak; the frequency where this peak occurs is the resonance frequency. Process 2) requires more complicated and expensive equipment; the question is whether the results provide an advantage that might make the investment worthwhile. The goal of this paper is to characterize the advantages and disadvantages of each approach, and thus enable informed decision-making about which approach to use.

2 Background and notation

2.1 Scattering

We transmit, from a single sensor, a known signal $f(t)$. The field thus produced propagates towards an unknown stationary object, scatters from it, and propagates back to the same sensor. This sensor measures the scattered field. We denote by $\mathbb{S}$ the operator that maps f to the (noiseless) received signal. This time-domain scattering operator can be represented as $\mathbb{S}f = \mathcal{S} * f = \int \mathcal{S}(t-t')f(t')dt'$, where $\mathcal{S}$ is the impulse response. The received signal, which includes noise n, is $\mathbb{S}f + n$.

2.2 The time-reversal operation

We denote by $\mathbb{T}$ the operation $(\mathbb{T}f)(t) = f^*(-t)$, where the star denotes complex conjugate. (Reasons for considering a complex-valued signal are given in Section 2.4.) For real-valued signals, $\mathbb{T}$ is simply time reversal. We note that $\mathbb{T}^2 = \mathbb{I}$ where $\mathbb{I}$ denotes the identity operator.

2.3 The frequency domain

We use the physics convention for the Fourier transform, *i.e.*, $F(\omega) = \int e^{i\omega t} f(t)dt$. The corresponding frequency-domain scattering operator is simply multiplication by the transfer function S, where $S(\omega) = \int e^{i\omega t}\mathcal{S}(t)dt$. Thus the frequency-domain received signal, which includes (frequency-domain) noise N, is $SF + N$.

In this document, we assume that the noise N is normally distributed with mean 0 and variance σ^2.

In the frequency domain, the operation $\mathbb{T}$ becomes

$$TF(\omega) = \int e^{i\omega t}(\mathbb{T}f)(t)dt = \int_{-\infty}^{\infty} e^{i\omega t} f^*(-t)dt = \int_{-\infty}^{\infty} e^{-i\omega t} f^*(t)dt = F^*(\omega) \quad (2.1)$$

and consequently $TST = S^*$, where the star denotes complex conjugate. Thus

$$(ST)^{2n} = (SS^*)^n \qquad \text{and} \qquad (ST)^{2n+1} = ST(SS^*)^n. \quad (2.2)$$

2.4 The analytic signal

In experiments we transmit and receive only real-valued signals f. The Fourier transforms of real-valued signals however, satisfy $F(-\omega) = F^*(\omega)$, which means that the information on the negative frequency axis is redundant. In the radar community, the convention is to delete the negative frequencies, which means that the corresponding time-domain signal, which is called the *analytic signal* [8], is complex valued. By the Paley-Wiener theorem, the analytic signal is indeed analytic in the upper half-plane in t. Chopping off the negative frequencies corresponds, in the time domain, to applying the Hilbert transform.

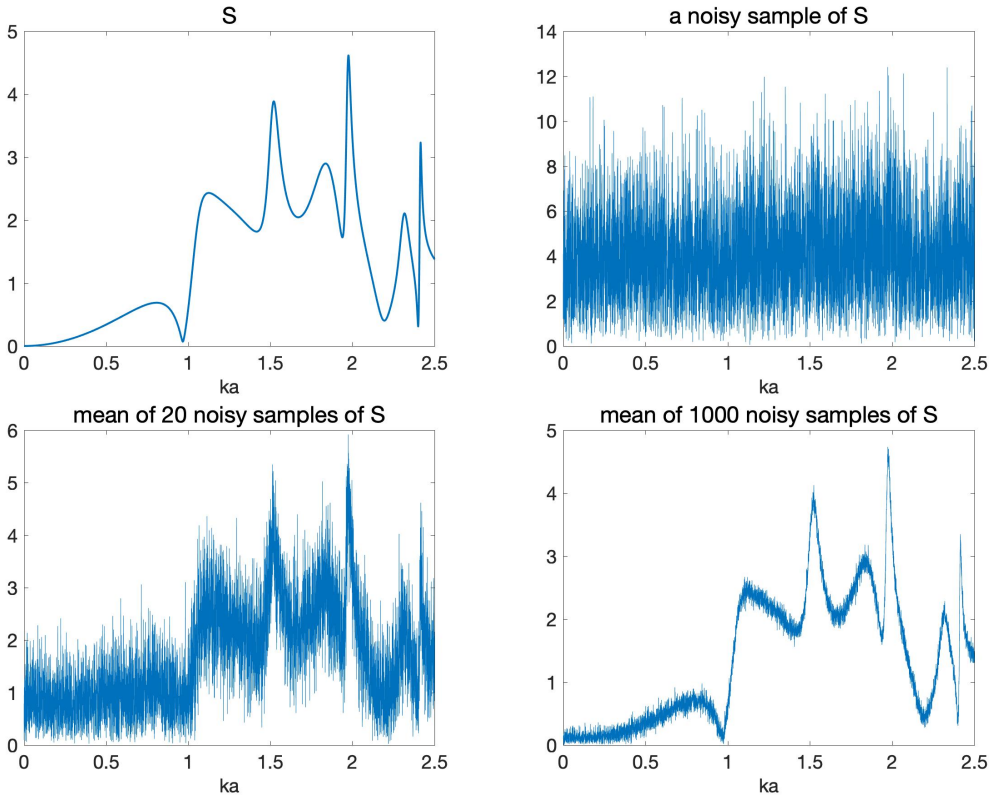

Figure 1: Top left: magnitude of noiseless scattering transfer function for electromagnetic scattering from a dielectric sphere. Top right: a normalized version of the same transfer function with added noise. Bottom: mean of 20 and 1000 such noisy transfer functions, respectively.

2.5 Averaging example

Fig. 1 shows the transfer function for a dielectric sphere. The noiseless scattering operator is shown on the top left plot of Fig. 1. The top right plot of Fig. 1 shows $\hat{S} = (S\tilde{F} + N)/\tilde{F}$, where $\tilde{F}$ is the initial waveform $F \equiv 1$ divided by the maximum of the real part of its Fourier transform. Here the additive noise is in $\mathcal{CN}(0, .0005)$. The bottom plots of Fig. 1 shows the average of 20 and 1000 such samples of $\hat{S} = (S\tilde{F}+N)/\tilde{F}$. The conclusion from Fig. 1 is that the mean of sufficiently many noisy measurements can give a good approximation to the transfer function. This is in line with the understanding that averaging N measurements typically reduces the effect of noise by $\sqrt{N}$.

3 The two procedures without normalization

We refer to the two procedures outlined in the Introduction as 1) averaging and 2) time reversal (TR).

3.1 Averaging

In the averaging approach, we make M measurements with a broadband signal F. The result of the mth measurement is $SF + N_m$. For the scalar case (*i.e.*, only one sensor), we use this measurement to estimate S as $\hat{S}_m = S + N_m/F$, where we have assumed that F is nonzero.

In the appendix, we show that to estimate S from multiple measurements S_m, $m = 1, 2, \ldots, M$, we compute the sample mean of the measurements

$$\hat{S} = \frac{1}{M}\sum_m \hat{S}_m = \frac{1}{M}\sum_m \left(S + \frac{N_m}{F}\right) = S + \frac{1}{FM}\sum_m N_m. \tag{3.1}$$

This averaging process decreases the standard deviation of the noise by a factor of $\sqrt{M}$. To mimic M iterations of the time-reversal procedure, we can then raise this sample mean to the power M, obtaining

$$|\hat{S}|^M = \left|S + \frac{1}{FM}\sum_m N_m\right|^M. \tag{3.2}$$

3.2 Time reversal without normalization

After one scattering operation, the received signal is $SF + N_1$.
After time-reversal and re-transmission, the received signal at the second iteration is $ST(SF + N_1) + N_2 = STSF + STN_1 + N_2$.
At the third iteration the received signal is $ST[ST(SF + N_1) + N_2] + N_3 = SS^*SF + SS^*N_1 + STN_2 + N_3$

Expected values. After one measurement, the expected value of the received signal is $\mathbb{E}(SF + N_1) = SF + \mathbb{E}N_1 = SF$.
After two measurements, the expected value is $\mathbb{E}(STSF + STN_1 + N_2) = STSF + ST\mathbb{E}N_1 + \mathbb{E}N_2 = STSF$.
After three measurements, the expected value is $\mathbb{E}\left[ST[ST(SF + N_1) + N_2] + N_3\right] = STSTSF$. We see that when the noise has zero mean, M iterations of the time-reversal process is expected to provide us with an unbiased estimate of $(ST)^M SF$.

Note that this discussion omits the normalization process. Normalization, which makes the process nonlinear, is discussed below in Section 4. Without normalization, the TR process can accommodate arbitrarily much noise. But this is because the transmitted energy can increase without bound as the number of iterations increases.

4 Time reversal with normalization

There are different ways that the transmitted energy can be constrained. The first is natural from a mathematical point of view, but less natural in experiments.

4.1 Normalization by energy

After one scattering operation, the received signal is $SF + N_1$. The L^2 norm is $\|SF + N_1\|$, so the new waveform is $T(SF + N_1)/\|SF + N_1\|$. Here the order of operations doesn't matter, because the norm is a scalar, so the time-reversal operation operates only on the numerator.

After the second scattering operation, the received signal is

$$\frac{ST(SF + N_1)}{\|SF + N_1\|} + N_2 = \frac{STSF + STN_1}{\|SF + N_1\|} + N_2. \tag{4.1}$$

Its norm is $\left\| ST(SF+N_1)/\|SF+N_1\| + N_2 \right\|$; consequently after the third scattering operation, the received signal is

$$\begin{aligned} ST\frac{\frac{STSF+STN_1}{\|SF+N_1\|} + N_2}{\left\| \frac{STSF+STN_1}{\|SF+N_1\|} + N_2 \right\|} + N_3 &= \frac{\frac{STSTSF+STSTN_1}{\|SF+N_1\|} + STN_2}{\left\| \frac{STSF+STN_1}{\|SF+N_1\|} + N_2 \right\|} + N_3 \\ &= \frac{STSTSF + STSTN_1 + \|SF + N_1\|STN_2}{\left\| STSF + STN_1 + \|SF + N_1\|N_2 \right\|} + N_3 \end{aligned} \tag{4.2}$$

It seems difficult to compute the expected value of these quantities. We note that the time-domain and frequency-domain L^2 norms are the same, so this process could equally well be written in the time domain.

4.2 Normalization by magnitude and time-gating

In practice, a much easier way to limit the energy is to limit the signal amplitude and duration.

Consequently we introduce a time-gating operator $\mathbb{X}$, defined by $(\mathbb{X}f)(t) = \chi(t)f(t)$ for some function χ that is zero outside some time interval $[-\tau, \tau]$. In the simulations reported below, this function is a characteristic function (1 inside the time interval and 0 outside). In the frequency domain, this time-gating operator is $\mathcal{X}F = X * F$, where X denotes the Fourier transform of χ and $*$ denotes convolution.

With time-gating, the time-reversal process is as follows. After one scattering operation, the frequency-domain received signal is $SF + N_1$, which in the time domain is $\int \mathcal{S}(t-t')f(t')dt' + n_1(t)$. We time-gate to obtain $\chi(t)\left[\int \mathcal{S}(t-t')f(t')dt' + n_1(t)\right]$. In the frequency domain this is $\mathcal{X}(SF+N_1)$. We then normalize by the time-domain maximum $\|\chi(\mathcal{S} * f) + \chi n_1\|_\infty$. We time-reverse and scatter again; thus as the next step we obtain, in the frequency domain,

$$ST\frac{\mathcal{X}(SF + N_1)}{\|\chi(\mathcal{S} * f) + \chi n_1\|_\infty} + N_2 \tag{4.3}$$

In the time domain, this is

$$\frac{\int \mathcal{S}(t-t')\chi(-t')\left[\int \mathcal{S}(-t'-t'')f(t'')dt'' + n_1(-t')\right]dt'}{\|\chi(\mathcal{S} * f) + \chi n_1\|_\infty} + n_2(t). \tag{4.4}$$

Table 1: Statistics for 200 4-measurement trials. The true value of the resonance is $ka = 1.9754$.

	Coherent averaging	TR
mean of estimates of ka	1.7819	1.9764
variance	0.0671	1.2544×10^{-5}
RMS error	0.3229	0.0037

Fig. 2 shows result of limiting the waveform duration as well as normalizing by the maximum of the real part. The duration limiting is done by simply chopping the waveform. Again the added noise, which is added after normalization, is in $\mathcal{CN}(0, .0005)$. Here the left column shows the averaging process for 2, 4, and 7 measurements. The right column shows the results of 2, 4, and 7 TR iterations. We note that again the largest peaks in the left column are not at the main resonance; clearly, at this level of noise, averaging 7 measurements is inadequate.

The rest of this paper normalizes each TR iterate by limiting the waveform duration and dividing by the maximum magnitude of the real part. As we will see, this energy-limiting process effectively limits the attainable SNR for the TR process.

5 Comparisons between averaging and TR

In this section we compare estimates of the main resonance from averaging and TR. In both cases we determine the ka of the resonance as the value of ka at which the maximum occurs.

5.1 4-measurement averaging vs. TR

Figure 3 shows a comparison for 4 TR iterations vs. 4 samples coherently averaged and raised to the 4th power. Statistics for estimation of the largest resonance is shown in Table 1.

5.1.1 Behavior at different noise levels

We compared the time-reversal procedure to the averaging method, under different levels of additive noise, for the case when each process makes 4 measurements. For sufficiently large noise, both methods fail.

Results are shown in Table 1 for 200 trials when both methods make 4 measurements, for added noise (added after normalization) in $\mathcal{CN}(0, .0005)$.

5.2 RMS error: TR vs. different numbers of averages

The examples above show that TR gives superior results when results from the same number of measurements are compared. In this section we investigate larger

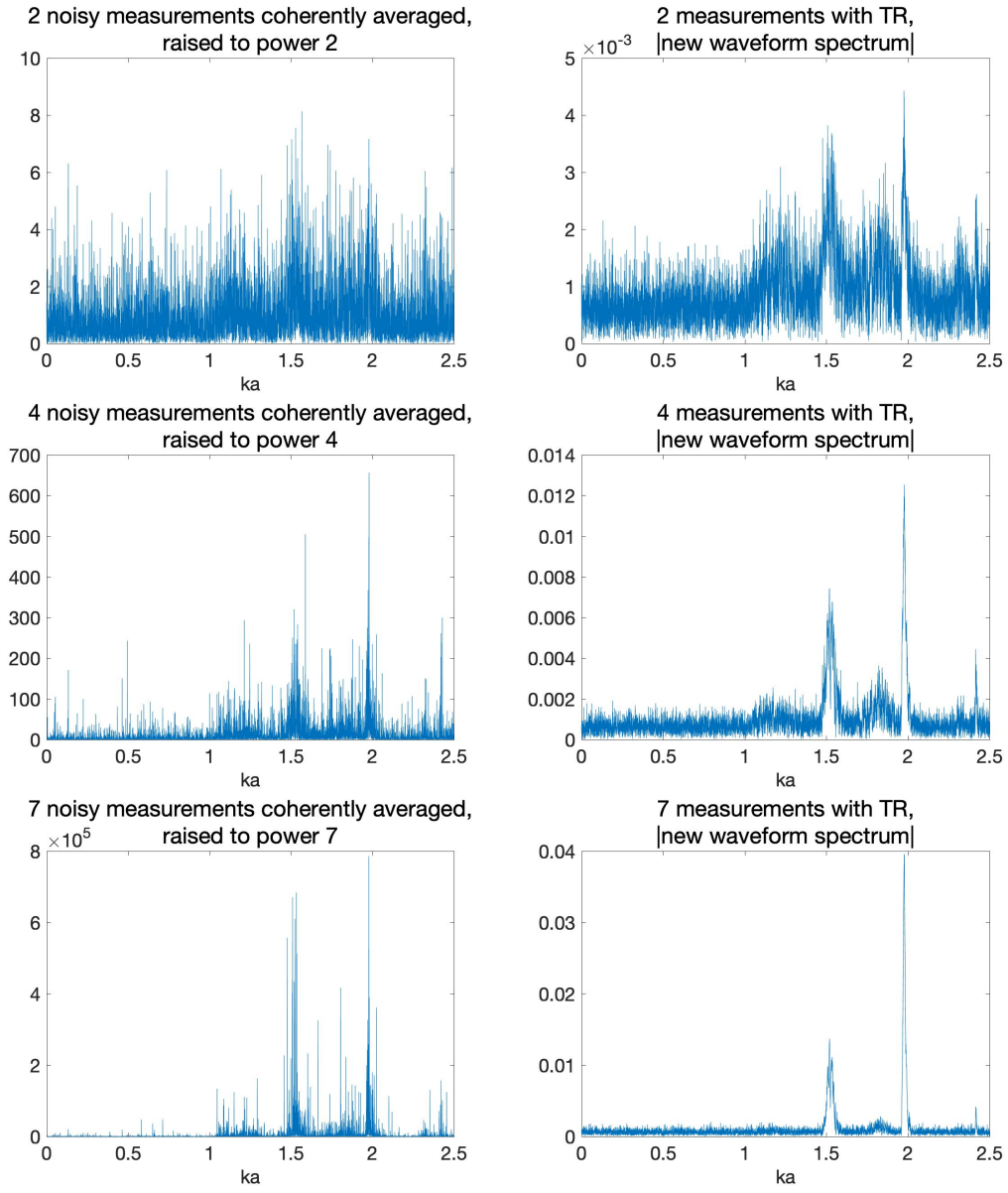

Figure 2: Limiting duration and normalizing by maximum: Comparison of the averaging process (left column) versus time-reversal (right column), after (rows) 2, 4, and 7 measurements.

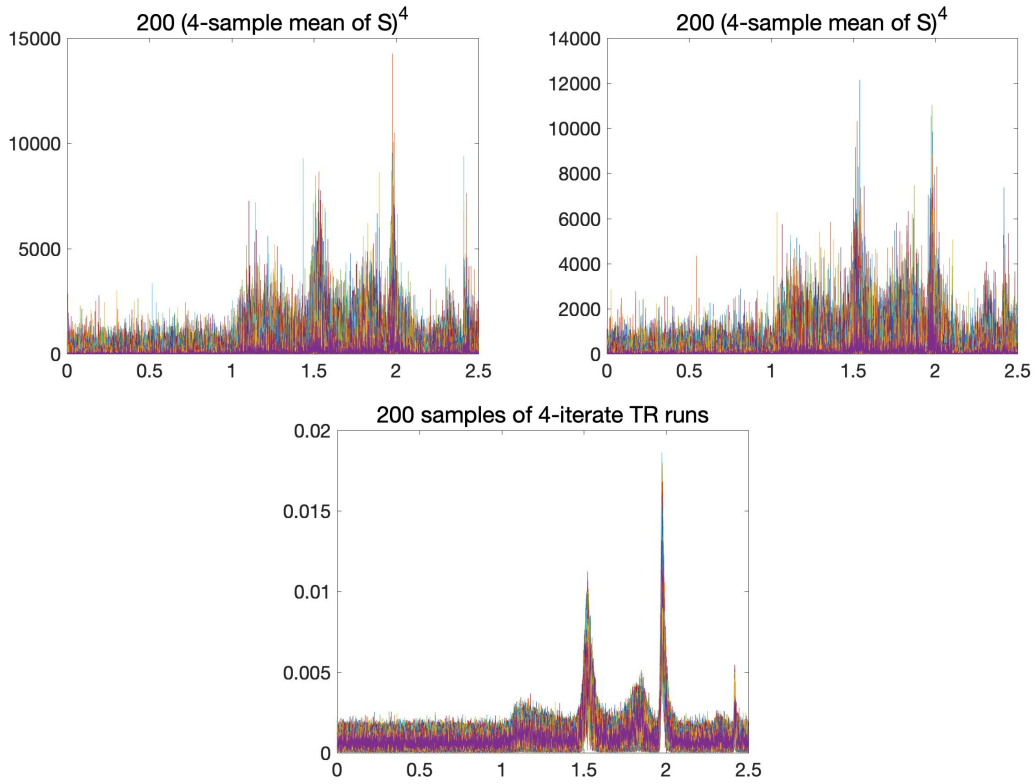

Figure 3: The top line shows two runs (with different realizations of noise) of 200 trials each for the averaging method with 4 measurements. The bottom plot shows 200 trials of a 4-iteration TR result. Different TR runs give indistinguishable results.

numbers of measurements for the averaging process.

Fig. 4 shows the RMS error in estimates of the resonance ka estimated by 4-iterate TR (heavy blue curve) for various numbers of averages ranging from 4 to 100 (light curves), as a function of noise level. The right plot is a zoomed-in version of the left plot (but with different realizations of noise). We note that the noise level for which TR fails is higher than that at which the averaging method fails, at least for averages of up to 100 samples.

The plateau region in the TR procedure for dielectric sphere arises because the secondary resonance is nearly as strong as the main resonance.

A case without such a nearby resonance is shown in Fig. 5, which corresponds to the case of a silver spherical nanoparticle at optical frequencies. The more isolated resonance produces no such extended plateau. Histograms for this case are shown in Fig. 10. In this case the correct peak is chosen consistently.

In Fig. 6 the left plot compares 1000 averages (heavy blue curve) to 10 TR iterations. The right plot shows 10 TR iterations (heavy blue curve) compared to a sampling of averages from 10 to 1000. These plots show results from 200 trials. Fig. 7 shows the estimated values of ka for the averaging method for each trial and each number of averages.

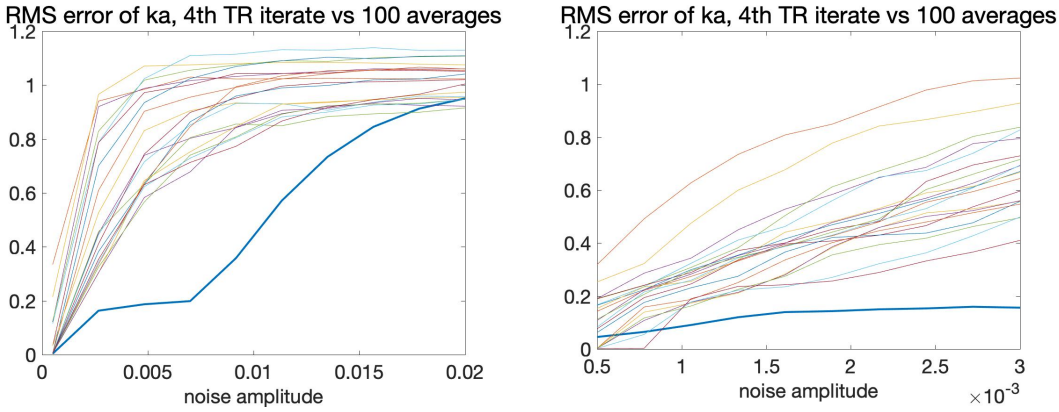

Figure 4: RMS error in estimate of ka, comparing various numbers of averages (light curves) vs 4-iterate TR (heavy blue curve), for different noise levels. The left plot is for the dielectric sphere; the right plot shows a zoomed plot near the origin.

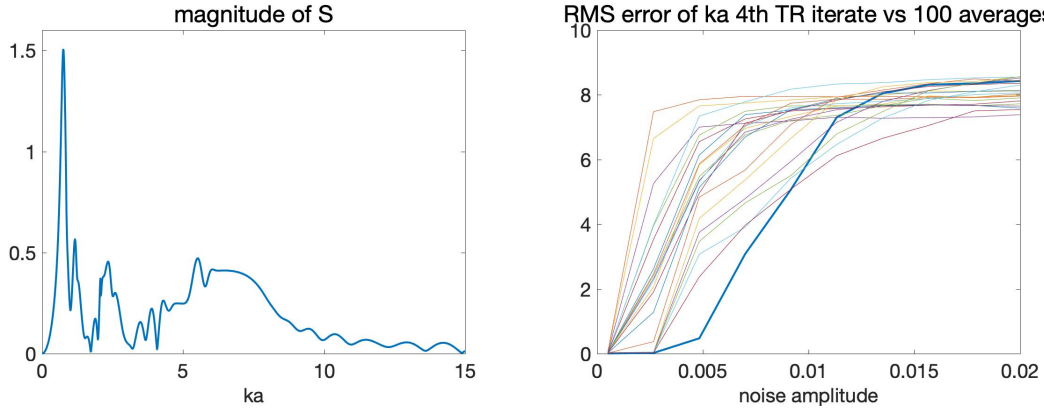

Figure 5: The left plot is the magnitude of the transfer function for a silver spherical nanoparticle at optical frequencies. Note the more isolated resonance. The right plot is the RMS error in estimate of ka, comparing various numbers of averages (light curves) vs 4-iterate TR (heavy blue curve), for different noise levels.

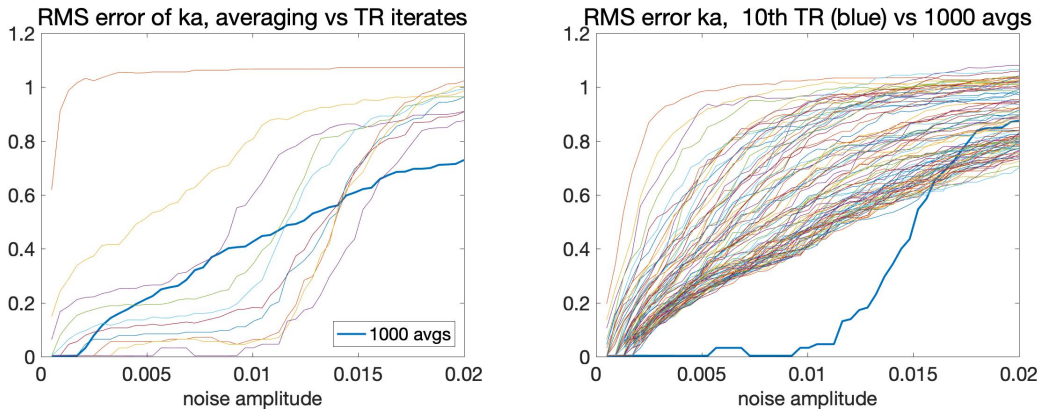

Figure 6: The RMS error of the estimates of ka for the largest resonance, as a function of the amplitude of the additive noise. Left: 1000 averages (heavy blue curve) vs. 1 – 10 TR iterations (multiple light curves). Right: 10 TR iterations (heavy blue curve) vs. a sampling of averages from 10 to 1000 (multiple light curves). The heavy blue curve on the right is the same as the light curve on the left for the 10th TR iteration. Results are shown for 200 trials.

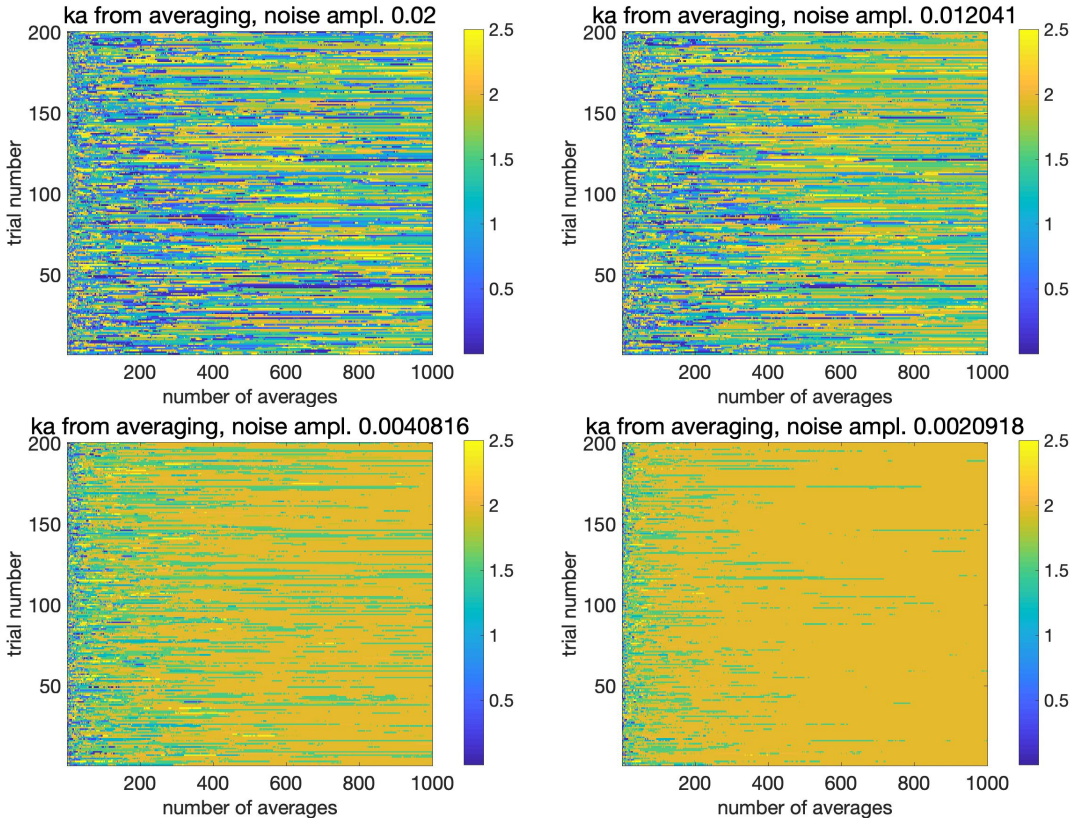

Figure 7: Estimated value of ka for the averaging method, for each trial and each number of averages, for decreasing noise amplitudes. The true value of ka corresponds to yellow.

5.3 Histograms

We can understand the behavior of TR more clearly in Fig. 8, which plots a histogram of ka estimates from TR as a function of noise amplitude. The color shows the fraction of the 200 trials that result in the estimate of ka marked on the vertical axis. Because every trial produces some estimate, the sum over each vertical slice is 1. Perfect performance would be a red bar at approximately $ka = 2$, stretching all the way across the plot. The length of the red bar indicates the level of noise at which the process fails.

We can understand the behavior of TR more clearly in Fig. 8, which plots a histogram of ka estimates from TR as a function of noise amplitude. The color shows the fraction of the 200 trials that result in the estimate of ka marked on the vertical axis. Because every trial produces some estimate, the sum over each vertical slice is 1.

We see that most of the trials produce the estimates of approximately 2, which is the correct value, but a significant fraction of trials return the estimate of about 1.5, which corresponds to the secondary peak in Fig. 1. Very few trials produce estimates other than these two numbers. Figure 9 shows the corresponding histograms for different numbers of averages.

Figure 10 and 11 show the TR and averaging histograms for the silver sphere, which has an isolated resonance at a value of ka less than 1.

5.4 SNR

The SNR is computed at the resonant frequency as the ratio of the mean of the magnitude squared divided by the variance. Fig. 12 shows improvement in SNR with TR iteration, for the cases of the dielectric sphere (left column) and silver sphere (right column). The top row shows the results starting with a broadband waveform, and the bottom row shows the “clairvoyant" results in which the iterations start with the ideal waveform, namely a CW wave at the resonant frequency. In the top two plots, we note that the first TR iteration seems to bring significant improvement in SNR, and later TR iterations contribute less improvement. In the bottom two “clairvoyant" plots, in which the iterates begin with the ideal waveform, we see that the first measurement is better than later ones. This is because the later iterates become contaminated with noise.

5.5 TR saturation

Although we see that the TR process provides rapid gains against low levels of noise, we expect that TR cannot continue to improve as the noise levels increase. This is because the TR gains are due to moving the transmitted energy to the resonant frequency, but the available instantaneous energy is limited by the equipment capacity (and in the simulations by the amplitude-and-duration-limiting normalization process). The number of repetitions of the averaging process may be similarly limited by the available energy, since each average requires the application of more energy,

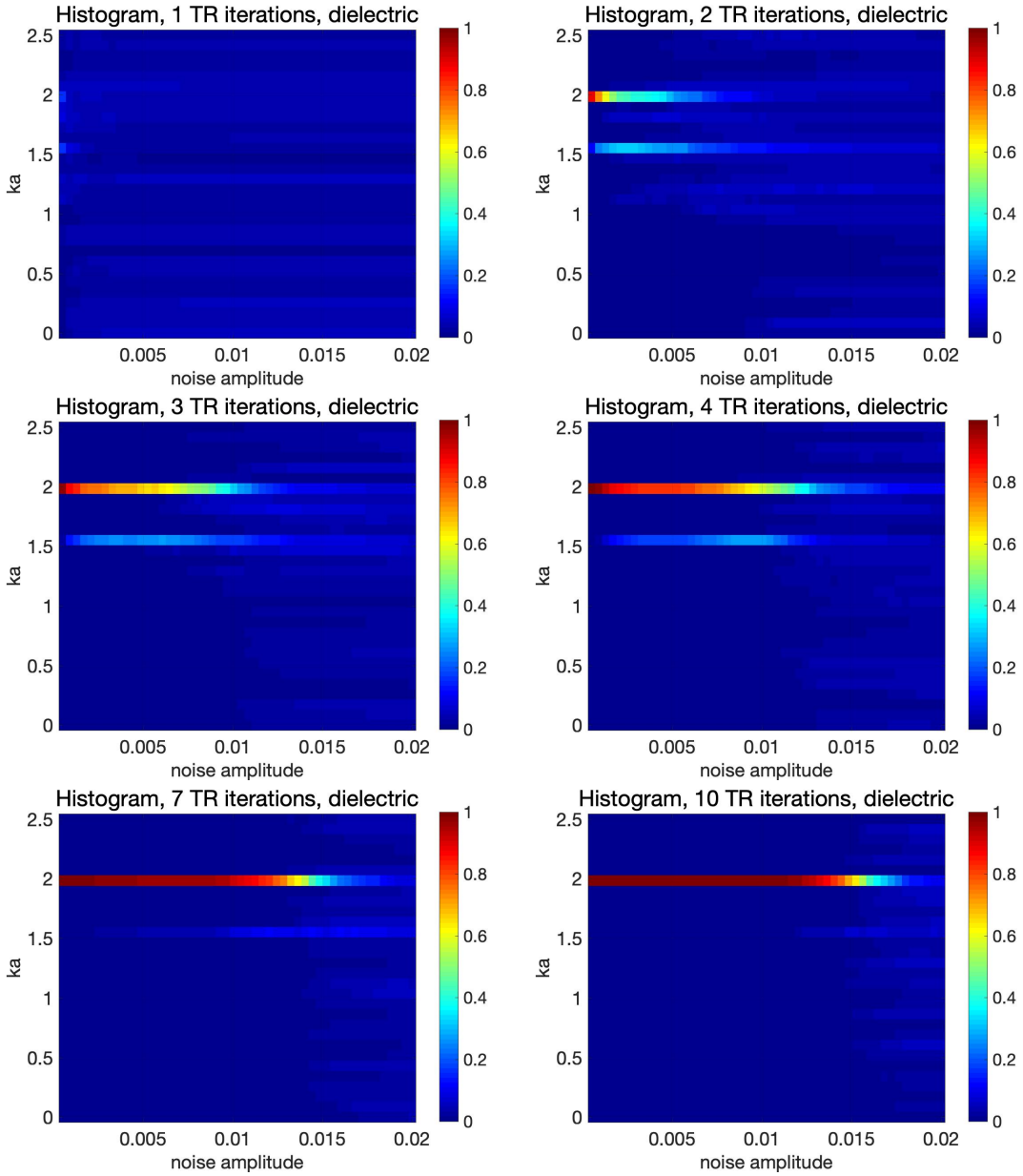

Figure 8: Histograms for TR iterates for the dielectric sphere. For each noise amplitude (horizontal axis), the color shows the fraction of trials that result in the estimate of ka marked on the vertical axis. The sum over every vertical slice is 1.

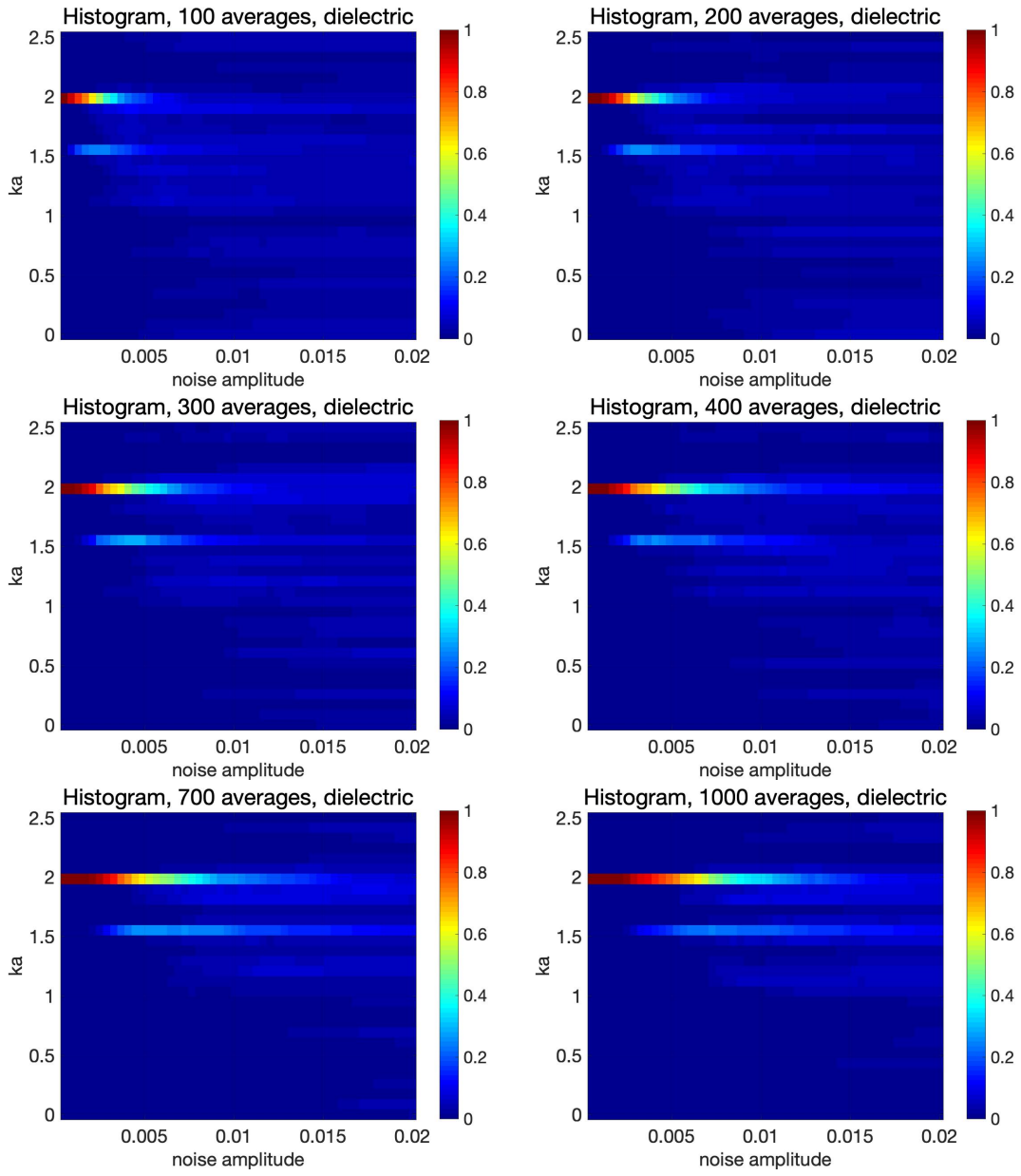

Figure 9: Histograms of ka estimates for different numbers of averages (100, 200, 300, 400, 700, 1000) for the dielectric sphere.

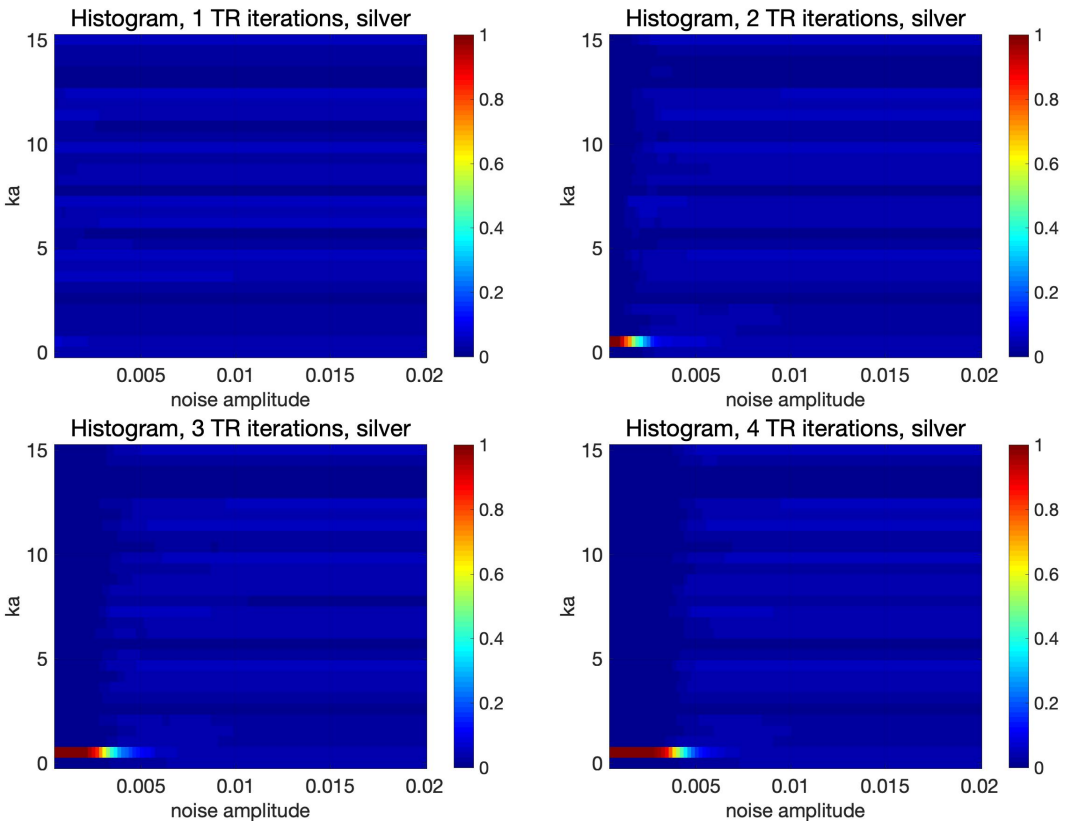

Figure 10: Histograms for TR iterates for the silver sphere. For each noise amplitude (horizontal axis), the color shows the fraction of trials that result in the estimate of ka marked on the vertical axis.

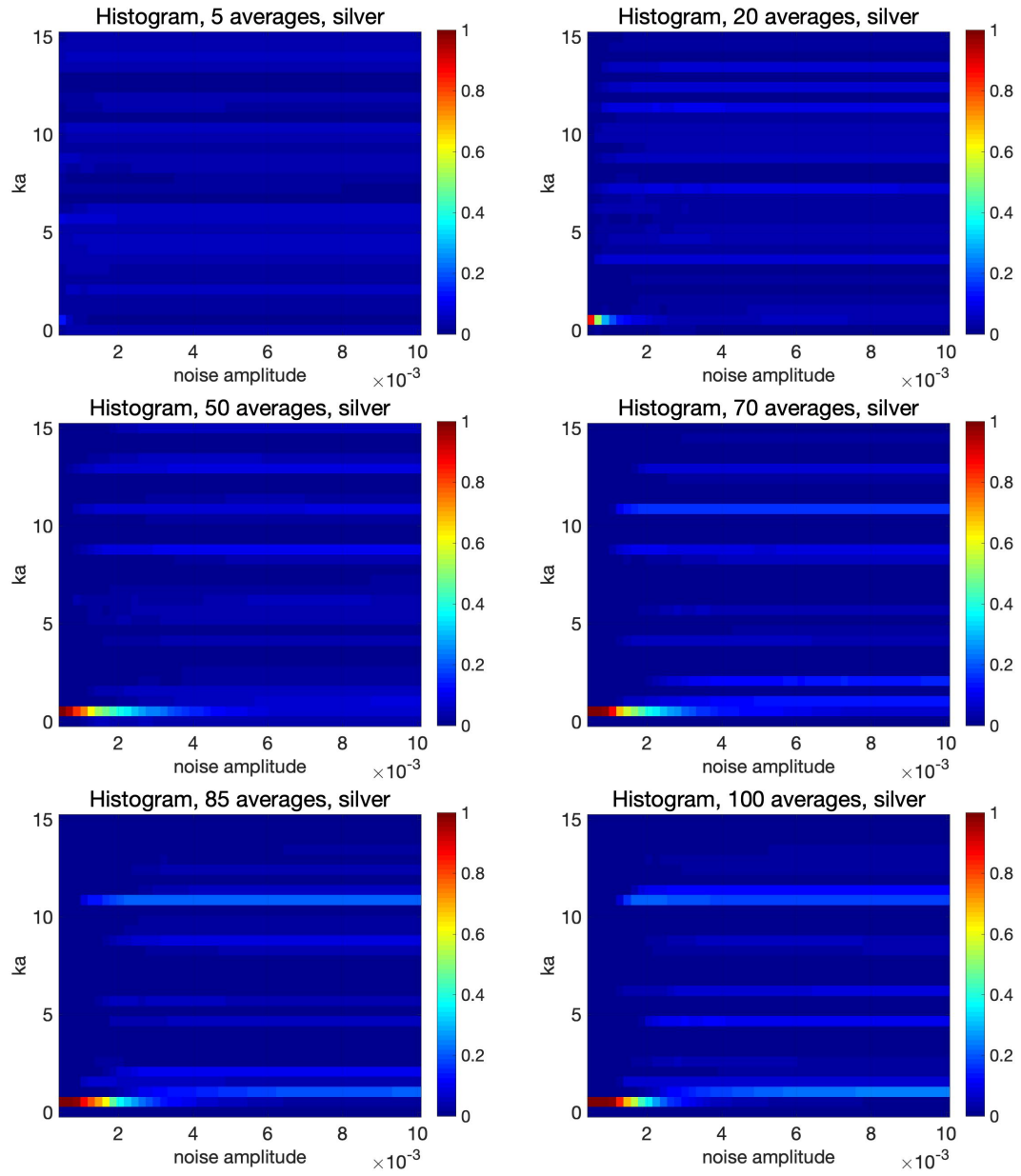

Figure 11: Histograms of ka estimates for different numbers of averages (5, 20, 50, 70, 85, 100) for the silver sphere.

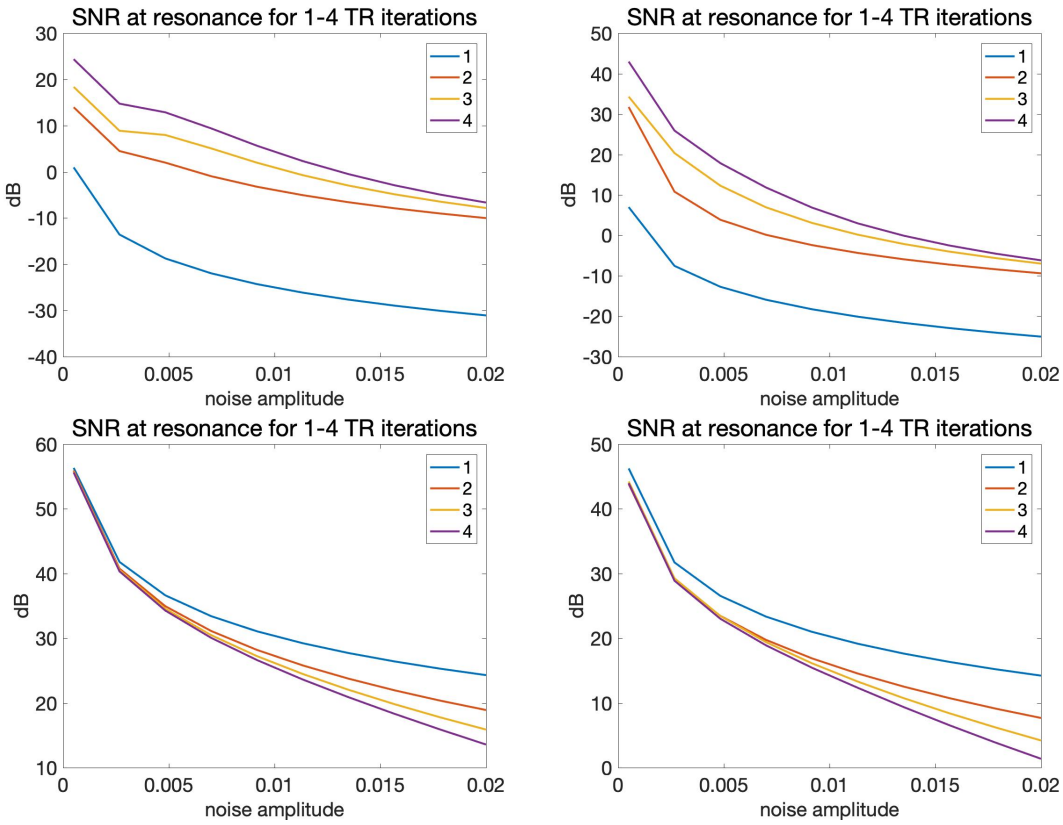

Figure 12: Signal-to-noise ratios for 4 TR iterates. Top row: starting with broadband waveform; Bottom row: starting with CW at resonant frequency. Left column: dielectric sphere; Right column: silver sphere. In all cases the initial measurement is the blue curve, the second red, third yellow, and fourth purple.

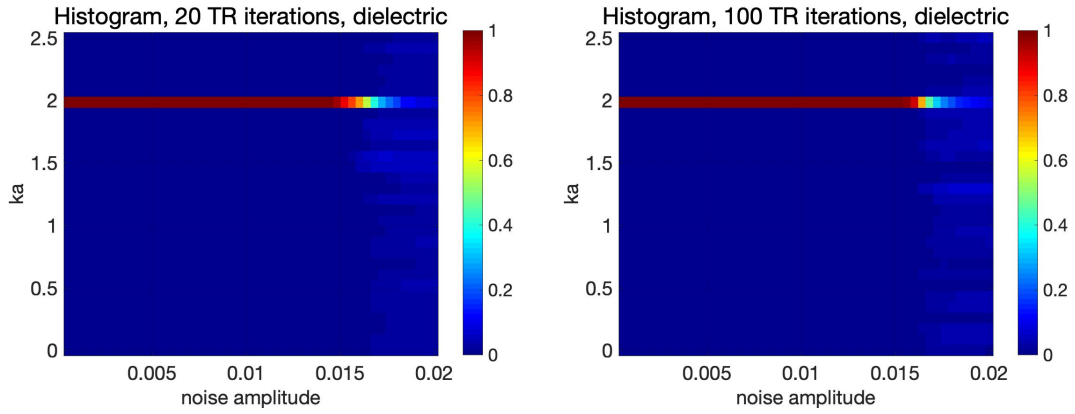

Figure 13: Histograms of ka estimates for large numbers TR iterations (20 and 100) for the dielectric sphere. The initial 10 iterations can be seen in Fig. 8.

but over the averaging process this energy is transmitted over a longer time period and not over a single pulse.

The saturation of the TR process is illustrated in Fig. 13. We see that little change occurs between 10 iterations (seen in Fig. 8) and 100 iterations (Fig. 13).

6 Conclusions

We found that when similar numbers of measurements are used, TR is noticeably better than averaging. The behavior in noise depends somewhat on the shape of the transfer function, particularly the presence or absence of resonances of nearly equal strength.

We showed that, compared to averaging, TR enables much quicker identification of resonances and uses fewer measurements. Moreover, it has a signal-to-noise advantage in the presence of limited additive receiver noise. However, TR is limited in the amount of noise it can handle.

The averaging method, on the other hand, has the advantages of being simpler and of not being limited in the amount of noise it can handle, if arbitrarily many measurements are allowed. This is because averaging suppresses noise.

An interesting approach might be to apply TR until its SNR saturates, save the result, repeat, and average the results. Or perhaps the TR process should apply averaging at each iteration. Perhaps the approach of [13] could be applied. Such investigations are left for the future.

7 Acknowledgments

This material[1] is based upon work that was supported in part by the Air Force Office of Scientific Research under awards FA9550-18-1-0087 and FA9550-21-1-0169 and by the Office of Naval Research under award number N00014-21-1-2145,

Appendix A Statistical estimation

This appendix recalls some basic facts about statistical estimation.

We assume that time-domain measurements are immediately converted into the frequency domain, so that we have an uncoupled problem of the form

$$Y_m(\omega) = X(\omega) + N_m(\omega),\ m = 1, 2, \dots M, \tag{A.1}$$

where the N_m are assumed to be independent and identically distributed complex Gaussian samples with mean 0 and variance σ^2. At each fixed frequency ω, from the M measurements of $Y_m,\ m = 1, 2, \dots M$, we want to estimate $X(\omega)$. Since the frequency is held fixed, we drop it from the notation.

The measurement column vector $\boldsymbol{Y}$ is distributed as

$$p(\boldsymbol{Y}) = \frac{1}{\pi \det(\Gamma)} e^{-(\boldsymbol{Y}-X\mathbf{1})^H \Gamma^{-1} (\boldsymbol{Y}-X\mathbf{1})} = \frac{1}{\pi M \sigma^2} e^{-|\boldsymbol{Y}-X\mathbf{1}|^2/\sigma^2} \tag{A.2}$$

where we have assumed that the covariance matrix Γ is of the form $\Gamma = \sigma^2 I$ with I the $M \times M$ identity matrix and where $\mathbf{1}$ is the column vector consisting of 1 in every entry. Here the superscript H denotes complex conjugate transpose.

A.1 Estimating by averaging

To obtain the maximum likelihood estimate of X from M measurements (A.1), we differentiate (A.2) with respect to X and X^* (complex conjugate) and set the derivatives to zero. We obtain $(\boldsymbol{Y} - X\mathbf{1})^* \cdot \mathbf{1} = 0$ and $\mathbf{1} \cdot (\boldsymbol{Y} - X\mathbf{1}) = 0$, which both result in the same maximum likelihood estimation formula

$$\hat{X} = \frac{1}{M} \sum_{m=1}^{M} Y_m \tag{A.3}$$

which shows that the maximum likelihood estimate of X is the sample mean of the measurements.

[1] Any opinions, findings, and conclusions or recommendations expressed in this material are those of the authors and do not necessarily reflect the views of the United States Air Force or Navy.

If the samples are of the form (A.1), then the variance of (A.3) is

$$\begin{aligned}\operatorname{Var}\hat{X} &= \mathbb{E}\left[\left(\frac{1}{M}\sum_{m=1}^{M} Y_m - X\right)^*\left(\frac{1}{M}\sum_{m'=1}^{M} Y_{m'} - X\right)\right] = \frac{1}{M^2}\mathbb{E}\left[\sum_m N_m^* \sum_{m'} N_{m'}\right] \\ &= \frac{1}{M^2} M\sigma^2 = \frac{\sigma^2}{M}\end{aligned} \tag{A.4}$$

In particular, if each measurement has mean X and standard deviation σ, then the average (A.3) of M measurements has mean X and standard deviation $\sigma/\sqrt{M}$. This shows that averaging suppresses noise.

A.2 Statistical estimation of the frequency of the largest resonance

For (A.1), the frequency at which $|X(\omega)|$ is largest is also the frequency at which it is easiest to distinguish between the two hypotheses

$$\begin{aligned}\mathbb{H}_1: &\quad \boldsymbol{Y}(\omega) = X(\omega)\mathbf{1} + \boldsymbol{N}(\omega) \\ \mathbb{H}_0: &\quad \boldsymbol{Y}(\omega) = \boldsymbol{N}(\omega)\end{aligned} \tag{A.5}$$

This is the frequency at which the log likelihood ratio $L(\omega)$ is maximized:

$$\begin{aligned}L(\omega) &= \log\frac{p_{\mathbb{H}_1}(\omega)}{p_{\mathbb{H}_0}(\omega)} = \log\frac{e^{-|\boldsymbol{Y}-X\mathbf{1}|^2/\sigma^2}}{e^{-|\boldsymbol{Y}|^2/\sigma^2}} = \frac{|\boldsymbol{Y}|^2}{\sigma^2} - \frac{|\boldsymbol{Y}-X\mathbf{1}|^2}{\sigma^2} \\ &= \frac{1}{\sigma^2}\left(\boldsymbol{Y}^*\cdot X\mathbf{1} + X^*\mathbf{1}\cdot\boldsymbol{Y} - |X|^2\underbrace{\mathbf{1}\cdot\mathbf{1}}_{M}\right)\end{aligned} \tag{A.6}$$

In (A.6), we use the maximum likelihood estimate (A.3), and $\mathbf{1}\cdot\boldsymbol{Y} = \sum_j Y_j$, obtaining

$$\begin{aligned}L(\omega) &\propto \left(\frac{1}{M}\sum_{m=1}^{M} Y_m\right)\left(\sum_j Y_j\right)^* + \left(\frac{1}{M}\sum_{m=1}^{M} Y_m\right)^*\left(\sum_j Y_j\right) - M\left|\frac{1}{M}\sum_{m=1}^{M} Y_m\right|^2 \\ &= \left|\frac{1}{M}\sum_{m=1}^{M} Y_m(\omega)\right|^2\end{aligned} \tag{A.7}$$

which is the same result we would have obtained by taking the magnitude squared of (A.3).

References

[1] C. E. Baum, *On the singularity expansion method for the solution of Electromagnetic Interaction Problems.* Kirtland AFB USASF, December 1971, vol. Interaction Notes #88.

[2] C. E. Baum, "Toward an engineering theory of electromagnetic scattering: The singularity and eigenmode expansion methods," in *Electromagnetic Scattering*, P. L. E. Uslenghi, Ed. Academic Press, 1978, ch. 13, pp. 571–651.

[3] C. Baum, E. Rothwell, Y. Chen, and D. Nyquist, "The singularity expansion method and its application to target identification," *Proceedings of the IEEE*, vol. 79, no. 10, pp. 1481–1492, October 1991.

[4] D. Chambers and J. Berryman, "Target characterization using decomposition of the time-reversal operator: electromagnetic scattering from small ellipsoids," *Inverse Problems*, vol. 22, no. 6, p. 2145, 2006.

[5] M. Cheney, D. Isaacson, and M. Lassas, "Optimal acoustic measurements," *SIAM J. Appl. Math.*, vol. 61, no. 5, pp. 1628–1647, 2001.

[6] M. Cheney and G. Kristensson, "Optimal electromagnetic measurements," *J J. Electromagnetic Waves and Applications*, vol. 15, no. 10, pp. 1323–1336, 2001. [Online]. Available: http://dx.doi.org/10.1163/156939301X01228

[7] E. Cherkaeva and A. Tripp, "On optimal design of transient electromagnetic waveforms," in *Expanded Abstracts, 67th Ann. Meeting, Soc. Exploration Geophys*, 1997, pp. 438–441.

[8] L. Cohen, Time-frequency analysis, Vol. 778. Prentice hall, 1995.

[9] C. Dolph and S. Cho, "On the relationship between the singularity expansion method and the mathematical theory of scattering," *IEEE Trans. Antennas Propagat.*, vol. 28, no. 6, pp. 888–897, November 1980.

[10] M. Fink, "Time reversal of ultrasonic fields. I. basic principles," *IEEE Trans. Ultrason., Ferroelect., Freq. Control*, vol. 39, no. 5, pp. 555–566, September 1992.

[11] M. Fink, "Time-reversed acoustics," *Scientific American*, vol. 281, no. 5, pp. 91–97, November 1999.

[12] M. Fink and C. Prada, "Topical review: Acoustic time-reversal mirrors," *Inverse Problems*, vol. 17, pp. R1–R38, 2001.

[13] M. Hardt and E. Price, "The noisy power method: A meta algorithm with applications," *Advances in neural information processing systems*, vol. 27, 2014.

[14] M. Hurst and R. Mittra, "Scattering center analysis via Prony's method," *IEEE Trans. Antennas & Propagation*, vol. 35, no. 8, pp. 986–988, August 1987.

[15] Y. Jin and J. Moura, "Time-reversal detection using antenna arrays," *IEEE Trans. Signal Processing*, vol. 57, no. 4, pp. 1396–1414, April 2009.

[16] I. Kirsteins, and A. Tesei, "Study of robustness of single-element-mirror time reversal method to reverberation and clutter: Simulations and tank measurements," In *Proc. of the Underwater Acoustic Measurements: Technologies and Exhibition conference*, Nafplion, Greece, p. 349, 2009.

[17] G. Kristensson, M. Cheney, and J.T. Kim, "Resonance Enhancement with Antenna Modeling", Lund University Technical Report LUTEDX/(TEAT-7261)/1-28/(2018); Vol. TEAT-7261, 2018

[18] T. Lobos and J. Rezmer, "Spectral estimation of distorted signals using Prony method," *Spectrum*, vol. 6, p. 7, 2003.

[19] L. Marin, "Natural-mode representation of transient scattered fields," *IEEE Trans. Antennas Propagat.*, vol. AP-21, no. 6, pp. 809–817, November 1973.

[20] J. Moura and Y. Jin, "Detection by time reversal: Single antenna," *IEEE Trans. Signal Processing*, vol. 55, no. 1, pp. 187–201, January 2007.

[21] C. Prada and M. Fink, "Eigenmodes of the time reversal operator: a solution to selective focusing in multiple-target media," *Wave Motion*, vol. 20, pp. 151–163, 1994.

[22] C. Prada, S. Manneville, D. Spoliansky, and M. Fink, "Decomposition of the time reversal operator: Detection and selective focusing on two scatterers," *J Acoust. Soc. Am.*, vol. 99, no. 4, pp. 2067–2076, 1996. [Online]. Available: http://scitation.aip.org/content/asa/journal/jasa/99/4/10.1121/1.415393

[23] A. G. Ramm, "Mathematical foundations of singularity and eigenmode expansion methods (SEM and EEM)," *J Math Anal Appl*, vol. 86, no. 86, pp. 562–591, 1982.

[24] T. K. Sarkar, S. Park, J. Koh, and S. Rao, "Application of the matrix pencil method for estimating the SEM (singularity expansion method) poles of source-free transient responses from multiple look directions," *IEEE Trans. Antennas Propagat.*, vol. 48, no. 4, pp. 612–618, April 2000.

[25] T. Sarkar and O. Pereira, "Using the matrix pencil method to estimate the parameters of a sum of complex exponentials," *IEEE Antennas Propag. Mag.*, vol. 37, no. 1, pp. 48–55, February 1995.